Preparation, Spectroscopic Characterization, and Theoretical Study of the $[Pd_4(dmb)_4(PPh_3)_2]Cl_2$ Complex (dmb = 1,8-Diisocyano-*p*-menthane) and Its Organometallic Polymer $\{[Pd_4(dmb)_5](CH_3CO_2)_2\}_n$: The First Examples of 58-Electron Linear Pd_4 Clusters

Tianle Zhang, Marc Drouin, and Pierre D. Harvey*

Département de chimie, Université de Sherbrooke, Sherbrooke, Québec J1K 2R1, Canada

Received September 28, 1998

The title compounds $[Pd_4(dmb)_4(PPh_3)_2]Cl_2$ (**1**) and $\{[Pd_4(dmb)_5](CH_3CO_2)_2\}_n$ (**2**) were prepared from the reactions $Pd_2(dba)_3{\cdot}CHCl_3$ + 2dmb + PPh_3 for **1** (dba = dibenzylideneacetone) and $Pd_2(dba)_3{\cdot}S$ + excess dmb + $Pd(O_2CCH_3)_2$ for **2** (S = benzene or $CHCl_3$), in good yields. The stuctures consist of quasi-linear Pd_4^{2+} species (d(PdPd) = 2.524(10), 2.524(10) and 2.534(10) Å for **1** and 2.5973(18), 2.6080(18), and 2.6080(18) Å for **2**) where the dmb ligands bridge the Pd atoms, forming a catenate. While the PPh_3 ligands axially coordinate the M_4 structure in **1**, a fifth dmb bridges another $Pd_4(dmb)_5^{2+}$ species, forming an organometallic polymer. From Raman spectroscopy, the two ν(PdPd) active modes (ν_1 and ν_2) are observed at 165 and 86 cm^{-1}, respectively, for **1** (F(PdPd) = 1.44 mdyn $Å^{-1}$). On the basis of EHMO (extended Hückel molecular orbital calculations), we predict that the HOMO and LUMO are the two dσ* orbitals arising from four interacting Pd atoms via the $d_{x^2-y^2}$, d_{z^2}, and p_x M atomic orbitals. This assignment is confirmed by the UV−vis spectra, in particular from the second-moment band analysis, which indicates that the two Franck−Condon active modes are modes with frequencies of 165 and 86 cm^{-1}, which are assigned to ν(PdPd). The compounds exhibit luminescence at 77 K with lifetimes in the microsecond regime. During the course of this study, use of $TCNQ^0$ (tetracyanoquinodimethane) as the oxidizing agent during the reaction (instead of $CHCl_3$ or $Pd(O_2CCH_3)_2$) leads to **3** ($[Pd_2(dmb)_4(\mu\text{-}Cl)](TCNQ)_3$), which is the first encapsulated halide ion "$M_2(dmb)_4$" species that is characterized from X-ray crystallography (d(PdCl) = 2.7143(6) Å). X-ray data for **2**·$4H_2O$: monoclinic, $P2_1/c$, a = 19.433(2) Å, b = 15.312(2) Å, c = 29.156(2) Å, β = 98.841(10)°, V = 8572.7(15) $Å^3$, Z = 4. X-ray data for **3**: triclinic, $P\bar{1}$, a = 13.314(2) Å, b = 13.490(2) Å, c = 14.645(2) Å, α = 108.267(10)°, β = 104.834(10)°, γ = 101.221(10)°, V = 2303.8(6) $Å^3$, Z = 1.

Introduction

The preparation of extended linear metallic chain compounds as new materials is a subject of current interest,[1] where some emphasis is given to solid-state materials that exhibit electric conductivity and optical properties.[2] Of all metallic complexes, the linear Pt_n species (where $n > 3$) represents a family of complexes that is very well explored.[3] However, for the non-M−M-bonded species that are not supported by bridging ligands, rapid chain dissociation occurs in solutions.[2a] There are some examples in the literature of bridged species which are X-ray crystallographically characterized and remain undissociated in solutions, notably for metals such as Cu(I) and Ag(I).[4] On the other hand, such chemistry is quasi-inexistent for Pd_n species. Rare examples include the shorter chain complexes $Pd_3(CNMe)_8^{2+}$ and $Pd_3(CNMe)_6(PPh_3)_2^{2+}$ [5] and the mixed-metal Pd_2Pt_2[3b] and M_2Pd_2 (M = Cr, Mo)[6] compounds. In the Pd_4 family, numerous cyclic compounds (of square or rectangular shapes) have been reported,[7] but to our knowledge, there is no known linear Pd_4 cluster so far. The only two other crystallographically characterized Pd_4 clusters exhibiting a 58 cluster valence electron count (CVE) have a butterfly $(Pd_4(CO)_5(PPh_3)_4)$[8] and a zigzag geometry $([Pd_4(\mu\text{-}Cl)_3(dppm)_2Cl_2]BF_4)$.[9]

* To whom correspondence should be addressed. Tel: (819) 821-8000, ext 2005. Fax: (819) 821-8017. E-mail: pharvey@courrier.usherb.ca.

(1) See, for instance: (a) Finniss, G. M.; Canadell, E.; Campana, C.; Dunbar, K. R. *Angew. Chem., Int. Ed. Engl.* **1996**, *35*, 2772. (b) Palmans, R.; MacQueen, D. B.; Pierpont, C. G.; Frank, A. J. *J. Am. Chem. Soc.* **1996**, *118*, 12647. (c) Shieh, S.-J.; Chou, C.-C.; Lee, G.-H.; Wang, C.-C.; Peng, S.-M. *Angew. Chem., Int. Ed. Engl.* **1997**, *36*, 56.

(2) (a) Miller, J. S. *Extended Linear Chain Compounds*; Plenum: New York, 1982; Vol. 1. (b) See, for instance: Pollagi, T. P.; Stoner, T. C.; Dallinger, R. F.; Gilbert, T. M.; Hopkins, M. D. *J. Am. Chem. Soc.* **1991**, *113*, 703.

(3) (a) Matsumoto, K.; Matsunami, J.; Urata, H. *Chem. Lett.*, ***1993***, 597. (b) Matsumoto, K.; Urata, H. *Chem. Lett.* **1993**, 2061. (c) Matsumoto, K.; Miyamae, H.; Moriyama, H. *Inorg. Chem.* **1989**, *28*, 2959. (d) O'Halloran, T. V.; Mascharak, P. K.; Williams, I. D.; Roberts, M. M.; Lippard, S. J. *Inorg. Chem.* **1987**, *26*, 1261. (e) Bernardinelli, G.; Castan, P.; Soules, R. *Inorg. Chim. Acta* **1986**, *120*, 205. (f) Laurent, J.-P.; Lepage, P.; Dahan, F. *J. Am. Chem. Soc.* **1982**, *104*, 7335. (g) O'Halloran, T. V.; Roberts, M. M.; Lippard, S. J. *J. Am. Chem. Soc.* **1984**, *106*, 6427. (h) Matsumoto, K.; Takahashi, H.; Fuwa, K. *J. Am. Chem. Soc.* **1984**, *106*, 2049. (i) Matsumoto, K. *Bull. Chem. Soc. Jpn.* **1985**, *58*, 651. (j) Matsumoto, K.; Fuwa, K. *Chem. Lett.* **1984**, 569. (k) Hollis, L. S.; Lippard, S. J. *Inorg. Chem.* **1993**, *22*, 2600. (l) Hollis, L. S.; Lippard, S. J. *J. Am. Chem. Soc.* **1983**, *105*, 3494. (m) Matsumoto, K.; Takahashi, H.; Fuwa, K. *Inorg. Chem.* **1983**, *22*, 4086. (n) Matsumoto, K.; Fuwa, K. *J. Am. Chem. Soc.* **1982**, *104*, 898. (o) Hollis, L. S.; Lippard, S. J. *J. Am. Chem. Soc.* **1982**, *103*, 1232. (p) Barton, J. K.; Szalda, D. J.; Rabinowitz, H. N.; Waszczak, J. V.; Lippard, S. J. *J. Am. Chem. Soc.* **1979**, *101*, 1434. (q) Barton, J. K.; Rabinowitz, H. N.; Szalda, D. J.; Lippard, S. J. *J. Am. Chem. Soc.* **1977**, *99*, 2827. (r) Barton, J. K.; Caravana, C.; Lippard, S. J. *J. Am. Chem. Soc.* **1979**, *101*, 7269. (s) Mascharak, P. K.; Williams, I. D.; Lippard, S. J. *J. Am. Chem. Soc.* **1984**, *106*, 6428.

(4) (a) Fortin, D.; Drouin, M.; Harvey, P. D. *J. Am. Chem. Soc.* **1998**, *120*, 5351. (b) Fortin, D.; Drouin, M.; Turcotte, M.; Harvey, P. D. *J. Am. Chem. Soc.* **1997**, *119*, 531. (c) Perreault, D.; Drouin, M.; Michel, A.; Harvey, P. D. *Inorg. Chem.* **1992**, *31*, 3688.

(5) (a) Balch, A. L.; Boehm, J. R.; Hope, H.; Alstead, M. M. *J. Am. Chem. Soc.* **1976**, *98*, 7431. (b) Clark, R. J. H.; Sourisseau, C. *Nouv. J. Chim.* **1980**, *4*, 287.

(6) (a) Mashima, K.; Tanaka, M.; Tani, K. *J. Am. Chem. Soc.* **1997**, *119*, 4307. (b) Mashima, K.; Nakano, H.; Nakamura, A. *J. Am. Chem. Soc.* **1996**, *118*, 9083. (c) Mashima, K.; Nakano, H.; Nakamura, A. *J. Am. Chem. Soc.* **1993**, *115*, 11632.

10.1021/ic9811594 CCC: $18.00
Published on Web 03/06/1999

We now wish to report the preparation, spectroscopic characterization, and EHMO theoretical study of the $[Pd_4(dmb)_4(PPh_3)_2]Cl_2$ complex (**1**) and its organometallic polymer $\{[Pd_4(dmb)_5](CH_3CO_2)_2\}_n$ (**2**). These are the very first examples of 58-electron linear Pd_4 clusters to be reported. Of particular interest, the dmb ligand has a very strong strong tendency to bridge bi-,[10] tri-,[11] and tetranuclear species[11,12] and, on some occasions, to encapsulate a metal cation such as Ag^+ [13] and halides (Cl^-, Br^-).[14,15] The title compounds are also the first examples where a catenate structure is observed with this ligand, a geometry that is rare in inorganic chemistry. During the course of this study, $TCNQ^0$ (neutral 7,7′,8,8′-tetracyanoquinodimethane) is used as the oxidizing agent for the reaction, instead of $CHCl_3$ or $Pd(O_2CCH_3)_2$, leading to the formation of the Cl^- encapsulated species $[Pd_2(dmb)_4Cl](TCNQ)_3$ (**3**). This compound represents the first complex where a halide ion is encapsulated inside a "$M_2(dmb)_4$" frame and is formally characterized from X-ray crystallography.

Experimental Section

Materials. $PdCl_2$ and PPh_3 (Aldrich) were used without further purification. $Pd_2(dba)_3{\cdot}C_6H_6$, $Pd_2(dba)_3{\cdot}CHCl_3$,[16] and dmb[17] were prepared according to standard procedures. All the experiments were carried out under N_2 atmosphere. Solvents for spectroscopic measurements were purified according to procedures outlined in ref 18.

Preparations. (a) $[Pd_4(dmb)_4(PPh_3)_2]Cl_2$ (1). 60.3 mg (0.0583 mmol) sample of $Pd_2(dba)_3{\cdot}CHCl_3$ was dissolved in 10 mL of acetone, and the solution was stirred under N_2(g) for 30 min. A 62.6 mg (0.3295 mmol) amount of dmb was dissolved in 5 mL of acetone, and this solution was added to the above solution also under N_2(g). The resultant solution turned red. After 52.2 mg (0.199 mmol) of PPh_3 was added, the color of the solution immediately changed from red to purple. The solution was allowed to stir for 2 h. Then the solution was filtered, and the filtrate was concentrated to about 2 mL. The purple product was collected by filtration and washed with diethyl ether. Yield: 46.7 mg (0.0262 mmol), 90%. Anal. Calcd for $Pd_4C_{84}H_{102}N_8P_2Cl_2$: C, 56.60; H, 5.77; N, 6.29. Found: C, 56.43; H, 5.90; N, 6.23. X-ray fluorescence measurements indicate that the relative amounts of Pd, P, and Cl are ~2.0, 1.0, and 1.0, respectively. ^{1}H NMR (CD_3CN), δ: 1.0−2.0 ppm (complex, 72H, dmb); 6.8−7.8 ppm (complex, 30H, PPh_3). ^{13}C NMR (CD_3CN), δ: 23.0, 27.3, 27.5, 28.2, 28.5, 37.3, 37.5, 44.6, 45.2, 60.8, 61.4, 62.9, 63.4 ppm (dmb); 128.8, 129.3, 130.5, and 133.8 ppm (PPh_3); 135.3, 135.5, 138.6, and 139.0 ppm (C≡). ^{31}P NMR (CD_3CN), δ: 9.1 ppm (s, fwhm ~2 ppm). FT-IR (solid): 2156 cm^{-1} (ν(N≡C)). FT-Raman (solid): 2185, 2148 cm^{-1} (ν(N≡C)); 165, 86 cm^{-1} (ν(PdPd)). Mass FAB, *m/e*: calculated for $Pd_4(dmb)_4(PPh_3)_2Cl$ 1746.9, observed 1748 (relative intensity <1%); calculated for $Pd_4(dmb)_4Cl$ 1222.3, observed 1222 (relative intensity = 100%). UV−vis (ethanol): λ_{max} (ϵ) 538 nm (53 700 M^{-1} cm^{-1}). Purple crystals were grown by diffusion of diethyl ether into dichloromethane solutions under N_2(g) atmosphere in the presence of a slight excess of dmb and PPh_3. Single crystals were obtained but were not of sufficient quality for complete X-ray structure determination. However, it was possible to demonstrate the isostructurality of the Pd_4^{2+} fragment with **2**.

(b) $\{[Pd_4(dmb)_5](CH_3CO_2)_2\}_n$ (2). A mixture of $Pd(O_2CCH_3)_2$ (0.0092 g, 0.041 mmol) and $Pd_2(dba)_3{\cdot}CHCl_3$ (0.0652 g, 0.063 mmol) was dissolved in 10 mL of acetone containing an excess of dmb (0.0632 g, 0.332 mmol). The solution was stirred under N_2 atmosphere for 4 h. The red solution was filtered, and the filtrate was concentrated to about 4 mL by rotary evaporator. A mixture of pentane and diethyl ether was used to precipitate the product. The bright orange product was collected by filtration and washed with pentane. Yield: 0.0586 g, 95%. IR (solid): 2152 cm^{-1} (ν(CN)); 1572, 1400 cm^{-1} ($\nu(CO_2^-)$). UV−vis (acetone + excess dmb): λ_{max} 512 nm. The dark-red crystals suitable for crystallography were grown by diffusion of pentane into a methyl ethyl ketone solution containing the orange product, also in the presence of excess dmb. $Pd_2(dba)_3{\cdot}C_6H_6$ can also be used as a starting material in this case.

(c) $[Pd_2(dmb)_4(\mu\text{-}Cl)](TCNQ)_3$ (3). To the suspension of $Pd_2(dba)_3{\cdot}CHCl_3$ (0.0425 g, 0.041 mmol) in 6 mL of acetone was added an excess of solid dmb (0.0406 g, 0.214 mmol), and the mixture was stirred under N_2 for 2 h. During the reaction, solid $Pd_2(dba)_3{\cdot}CHCl_3$ was dissolved, yielding a red solution. The mixture was filtered, and the filtrate was moved to a long tube. Then 0.0350 g (0.171 mmol) of $TCNQ^0$ dissolved in 8 mL of acetone followed by N_2 was added to the tube. The resulting green solution was left at room temperature. Purple crystals that formed overnight were collected by filtration and washed with acetone and diethyl ether. Yield: 0.0292 g (0.018 mmol), 66% based on Pd. Anal. Calcd for $C_{96}H_{88}N_{24}ClPd_2{\cdot}H_2O$: C, 62.52; H, 4.92; N, 18.23. Found: C, 62.70; H, 5.28; N, 18.17. IR: 2175 (br, vs), 2245 (m) cm^{-1} (ν(CN)). UV−vis (CH_3CN): λ_{max} 394, 680, 764, 760 nm. ^{1}H NMR (CD_3CN), δ: 1.45−1.75 (br, dmb, 72H), 2.0−2.3 (complex, TCNQ, 12H).

Instruments. The UV−visible spectra were recorded on a Hewlett-Packard 8452A diode array spectrometer. The chemical analysis measurements were performed at the Université de Montréal for C, H, and N and at the Université de Sherbrooke for Pd and Cl. In the latter case, the qualitative data were obtained using a KEVEX-700 X-ray emission spectrofluorometer operating at 60 kV. The mass spectra were acquired on a Kratos MS-50 TCTA spectrometer using an Iontech

(7) (a) Tanase, T.; Nomura, T.; Fukushima, T.; Yamamoto, Y.; Kobayashi, K. *Inorg. Chem.* **1993**, *32*, 4578. (b) Burrows, A. P.; Hill, C. M.; Mingos, D. M. P. *J. Organomet. Chem.* **1993**, *456*, 155. (c) Moiseev, I. I.; Stromnova, T. A.; Vargaftig, M. N.; Mazo, G. Ja.; Kuz'mina, L. G.; Struchkov, Yu. T. *J. Chem. Soc., Chem. Commun.* **1978**, 27. (d) Braunstein, P.; Luke, M. A.; Tiripicchio, A.; Tiripicchio Namellini, M. *Angew. Chem., Int. Ed. Engl.* **1987**, *26*, 768. (e) Mimoun, H.; Charpentier, R.; Mitschler, A.; Fisher, J.; Weiss, R. *J. Am. Chem. Soc.* **1980**, *102*, 1047. (f) Gauthron, I.; Gagnon, J.; Zhang, T.; Rivard, D.; Lucas, D.; Mugnier, Y.; Harvey, P. D. *Inorg. Chem.* **1998**, *37*, 1112. (g) Stromnova, T. A.; Busygina, I. N.; Katser, S. B.; Antsyshkina, A. S.; Porai-Koshits, M. A.; Moiseev, I. I. *J. Chem. Soc., Chem. Commun.* **1988**, 114.

(8) Felthan, R. D.; Elbaze, G.; Ortega, R.; Eck, C.; Dubrawski, J. *Inorg. Chem.* **1985**, *24*, 1503.

(9) Braunstein, P.; Luke, M. A.; Tiripicchio, A.; Tiripicchio Camellini, M. *New J. Chem.* **1988**, *12*, 429.

(10) (a) Perreault, D.; Drouin, M.; Michel, A.; Harvey, P. D. *Inorg. Chem.* **1992**, *31*, 2740. (b) Che, C.-M.; Herbstein, F. H.; Schaefer, W. P.; Marsh, R. E.; Gray, H. B. *Inorg. Chem.* **1984**, *23*, 2572. (c) Rhodes, M.; Mann, K. R. *Inorg. Chem.* **1984**, *23*, 2053. (d) Miskowski, V. M.; Rice, S. F.; Gray, H. B.; Dallinger, R. F.; Milder, S. J.; Hill, M. G.; Exstrom, C. L.; Mann, K. R. *Inorg. Chem.* **1994**, *33*, 2799. (e) Che, C.-M.; Wong, W.-T.; Lai, T.-F.; Kwong, H.-L. *J. Chem. Soc., Chem. Commun.* **1989**, 243. (f) Boyd, D. C.; Matsch, P. A.; Mixa, M. M.; Mann, K. R. *Inorg. Chem.* **1986**, *19*, 3331. (g) Perreault, D.; Drouin, M.; Michel, A.; Harvey, P. D. *Inorg. Chem.* **1993**, *32*, 1903. (h) Sykes, A. G.; Mann, K. R. *J. Am. Chem. Soc.* **1990**, *112*, 7247. (i) Harvey, P. D.; Murtaza, Z. *Inorg. Chem.* **1993**, *32*, 4721. (j) Gladfelter, W. L.; Gray, H. B. *J. Am. Chem. Soc.* **1980**, *102*, 5909. (k) Xiao, H.; Cheung, K. K.; Che, C.-M. *J. Chem. Soc., Dalton Trans.* **1996**, 3699.

(11) Harvey, P. D.; Drouin, M.; Michel, A.; Perreault, D. *J. Chem. Soc., Dalton Trans.* **1993**, 1365.

(12) The structure for the tetranuclear $[Ag_4(dmb)_4(TCNQ)_3]TCNQ$ complex will be reported in due course: Fortin, D.; Drouin, M.; Harvey, P. D.; Herring, F. G.; Summers, D. A.; Thompson, R. C. Submitted for publication.

(13) (a) Sykes, A. G.; Mann, K. R. *Inorg. Chem.* **1990**, *29*, 4449. (b) Sykes, A. G.; Mann, K. R. *J. Am. Chem. Soc.* **1988**, *110*, 8252.

(14) The reaction of $Pd_2(dmb)_2Cl_2$ with PPh_2Me in the presence of $NaPF_6$ leads to $[Pd_2(dmb)_2(PPh_2Me)_4(\mu\text{-}Cl)](PF_6)_3$ (Jourdan, N.; Drouin, M.; Harvey, P. D. Unpublished result) and a unidentified red product. From the X-ray structure, the Cl ion was encapsulated inside the two $Pd^{II}L_2L_2'$ fragments.

(15) (a) Gladfelter, W. L.; Gray, H. B. *J. Am. Chem. Soc.* **1980**, *102*, 5910. (b) Che, C.-M.; Herbstein, F. H.; Schaefer, W. P.; Marsh, R. E.; Gray, H. B. *Inorg. Chem.* **1984**, *23*, 2572.

(16) Takahashi, Y.; Ito, T.; Ishii, Y. *J. Chem. Soc., Chem. Commun.* **1970**, 1065.

(17) Weber, W. P.; Gokel, G. W.; Ugi, I. K. *Angew. Chem., Int. Ed. Engl.* **1972**, *11*, 530.

(18) (a) Perrin, D. D.; Armarego, W. L. F.; Perrin, D. R. *Purification of Laboratory Chemicals*; Pergamon: Oxford, U.K., 1966. (b) Gordon, A. J.; Ford, R. A. *The Chemist's Companion. A Handbook of Practical Data, Techniques, and References*; Wiley: New York, 1972; p 436.

model FAB 11NF saddle field source operating at 70 kV with 2 mA current. The samples were in thiolglycerol or NBA matrixes. The FT-IR (4000−600 cm^{-1}) spectra were obtained on a Bomem (MB-102) spectrometer. The Raman spectra at 298 K in the solid state were acquired using a Bruker IFS 66/CS FT-IR spectrometer coupled with an FRA 106 FT-Raman module using a Nd:YAG laser (1064 nm excitation) and a Notch filter (cutoff ∼50 cm^{-1}). The variable-temperature measurements were performed using a homemade assembly. The sample temperature, which was controlled by a cooled N_2(g) flow from the bottom to the top of a cylindrical quartz Dewar cell, was monitored using a calibrated gold−chromium thermocouple (with the temperature of an ice/water bath as the reference temperature) and was allowed to stabilize for 5 min prior to each measurement. The luminescence spectra were obtained on a steady-state LS-100 spectrofluorometer from Photon Technology Inc. or on a Fluorolog II instrument. The emission lifetimes were measured on the PTI LS-100 instrument using a nanosecond photon-counting system or a microsecond pulsed system.

Calculational Details. All of the MO calculations were of the extended Hückel type (EHMO)[19,20] using a modified version of the Wolfsberg−Helmohlz formula.[21] The atomic parameters used for C,[20] N,[20] H,[20] P,[22] and Pd[23] were from the literature. Because of limitations in the size of molecules handled by the program, dmb was replaced by two CH_3NC molecules and PPh_3 was replaced by PH_3. Hence, the computed ions are $Pd_4(CNMe_3)_8(PH_3)_2^{2+}$ and $Pd_4(CNMe)_{10}^{2+}$. This methodology is a standard one.[24a] The bond distances are those reported for the X-ray structures (average values). For **2**, $d(Pd_2) = 2.61$, $d(Pd-C)_{eq} = 2.00$, $d(Pd-C)_{ex} = 1.93$, $d(C\equiv N)_{ex} = 1.148$, and $d(C\equiv N)_{eq} = 1.34$ Å. For **1**, $d(Pd_2) = 2.53$ and $d(PdP) = 2.35$ Å as crystallographically determined (see below). The other distances were taken as $d(Pd-C) = 1.96$, $d(C\equiv N) = 1.138$, and $d(N-C) = 1.476$ Å (average values taken from other Pd−CNR species and **2**). All angles were 90 or 180° for an idealized structure unless stated otherwise due to the dihedral angle. The detailed description of the graphic programs used in this work can be found in ref 24b. The electronic spectral simulations were performed using Heller's time-dependent theory,[25] similar to that of a Franck−Condon analysis.

X-ray Crystallography. For $\{Pd_4(dmb)_5(CH_3CO_2)_2\}_n \cdot 4H_2O$, intensity data were collected at 180 K on an Enraf-Nonius CAD-4 automatic diffractometer using graphite-monochromated Cu Kα radiation. The DIFFRAC program was used for centering, indexing, and data collection. The unit cell dimensions were obtained by a least-squares fit of 10 centered reflections in the range $20° \le 2\theta \le 30°$. During data collection, the intensities of two standard reflections were monitored every 60 min. No significant decay was observed. An absorption correction was applied to the data based on ψ-scan measurements of nine azimutal reflections. The structure was solved by the application of direct methods using the SOLVER program from NRCVAX[26a,b] and refined by least-squares procedures using the SHELXL-97[26c] program. In the asymmetric unit, there are four water molecules. At convergence, the final discrepancy indices were $R = 0.0957$, $R_w = 0.2931$, and $S = 1.232$.[27] The residual positive and negative electron densities in the final maps were located in the vicinity of the Pd atoms. All non-H atoms were refined isotropically except for the Pd atoms. The H atoms were geometrically placed. The dmb ligands are disordered. The occupancy refinement converged to 0.598(12)/0.402(12), 0.704(12)/0.296(12), 0.732(12)/0.268(12), and 0.620(13)/0.380(13) ratios. The quality of the crystal combined with disorder prevented better refinement.

Chart 1

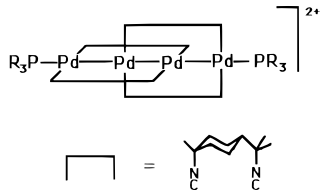

Results and Discussion

1. Preparation and X-ray Structure. The $d^{10}-d^{10}$ $Pd_2(dba)_3 \cdot CHCl_3$ dimer reacts with an excess of dmb and PPh_3 in acetone under inert atmosphere to give **1** in good yield (Chart 1). Reaction between $Pd_2(dba)_3 \cdot C_6H_6$ and dmb in excess provided a red luminescent solid which proved to be too unstable in both the presence and the absence of oxygen for characterization. Upon addition of PPh_3 to these reactions, similar products were obtained with improved stability, but no crystal suitable for X-ray crystallography was obtained. Finally, in the presence of a chlorocarbon, either from the starting $Pd_2(dba)_3 \cdot CHCl_3$ material or from added CH_2Cl_2, this reaction provided the oxidized purple species, **1**. Although **1** is relatively stable in the solid state, this cluster is readily unstable in solutions in the presence of air and slowly decomposes under inert atmosphere. The identitfication of this new compound was made possible with a combination of (1) X-ray data obtained for low-quality single crystals of **1**,[28,29] (2) detailed spectroscopic analysis (Experimental Section), and (3) comparison with X-ray data obtained for **2** (below). The presence of Cl^- ions was confirmed by chemical analysis and mass FAB analysis.

Similarly, $Pd_2(dba)_3 \cdot S$ ($S = CHCl_3$ or C_6H_6) reacts with $Pd(O_2CCH_3)_2$ in the presence of an excess of dmb under inert atmosphere, to form the organometallic polymer **2**. The X-ray structure (Figure 1; Tables 1 and 2) reveals a series of quasi-linearly Pd−Pd-bonded Pd_4^{2+} species linked by dmb ligands. These Pd_4^{2+} species are built upon two 20-membered ring "$Pd_2(dmb)_2^{+}$" fragments interlocked to form a catenate structure, where two dmb ligands bridge the first and third Pd metals and the other two bind the second and fourth. To our knowledge, these examples are unique. The Pd−Pd bond distances are 2.597(2) Å for the inner bond and 2.608(2) and 2.623(2) Å for the outer bonds, typical of Pd−Pd single bonds. The average Pd_3 angle is 174.5°, indicating a slight deviation from perfect

(19) Hoffmann, R.; Lipscomb, W. N. *J. Chem. Phys.* **1962**, *36*, 2179.
(20) (a) Hoffmann, R.; Lipscomb, W. N. *J. Chem. Phys.* **1962**, *36*, 2872. (b) Hoffmann, R. *J. Chem. Phys.* **1963**, *39*, 1397.
(21) Ammeter, J. H.; Burgi, H. B.; Thibeault, J. C.; Hoffmann, R. *J. Am. Chem. Soc.* **1978**, *100*, 3686.
(22) Summerville, R. H.; Hoffmann, R. *J. Am. Chem. Soc.* **1976**, *98*, 7240.
(23) Macchi, P.; Proserpio, D. M.; Sironi, A. *Organometallics* **1997**, *16*, 2101.
(24) (a) Mealli, C. *J. Am. Chem. Soc.* **1985**, *107*, 2245. (b) Mealli, C.; Proserpio, D. M. *J. Chem. Educ.* **1990**, *67*, 399.
(25) Heller, E. J. *Acc. Chem. Res.* **1981**, *14*, 368.
(26) (a) LePage, Y.; White, P. S.; Gabe, E. J. NRCCAD: An Enhanced CAD-4 Control Program. Proc. Am. Crystallogr., Hamilton, Canada, 1986; Abstract PA23. (b) Gabe, E. J.; LePage, Y.; Charland, J.-P.; Lee, F. L.; White, P. S. *J. Appl. Crystallogr.* **1989**, *22*, 384. (c) Sheldrick, G. SHELX-97. Universität Göttingen, Göttingen, Germany, 1997.
(27) (a) $R = \sum||F_o| - |F_c||/\sum|F_o|$. (b) $R_w = \{\sum[w(F_o^2 - F_c^2)^2]/\sum w(F_o^2)^2\}^{1/2}$ [$w = 1/[s^2(F_o^2) + (0.1P)^2$ where $P = (F_o^2 + 2F_c^2)/3$]. (c) $S = \{\sum[w(F_o^2 - F_c^2)^2]/(\text{no. of reflns} - \text{no. of params})\}^{1/2}$. (d) The ORTEP drawings were prepared using ORTEP: Johnson, C. K. ORTEP. In *Xtal_GX*; Hall, DuBoulay, Eds.; University of Western Australia: Nedlands, Australia, 1995.
(28) The reaction of $Pt_2(dba)_3 \cdot CHCl_3$ with dmb and PPh_3 provides $[Pt_4(dmb)_4(PPh_3)_2](Cl)_2$, which was formally characterized by X-ray crystallography (Zhang, T.; Drouin, M.; Harvey, P. D. *Inorg. Chem.* **1999**, *38*, 957). The isostructurality of this compound with **1** leaves no doubt. In this case, two water and two acetonitrile molecules crystallize within the unit cell.
(29) **1** crystallizes in a monoclinic cell (*A*2), with $a = 18.869(3)$ Å, $b = 23.234(3)$ Å, $c = 25.594(4)$ Å, $\beta = 108.420(20)°$, $V = 10646(3)$ Å^3, and $Z = 8$ for a formula of $Pd_2PN_4C_{32}Cl$ (fw = 719.60); $R = 0.148$, $R_w = 0.146$, and GOF = 7.76. The poor quality of the crystal prevented further analysis where only 3760 reflections were collected. The Pd−Pd distances are found to be somewhat typical for Pd^I-Pd^I single bonds with isocyanide ligands (2.534(13) Å, inner; 2.524(10) and 2.524(10) Å, outer). The Pd−C distances average 2.00 Å.

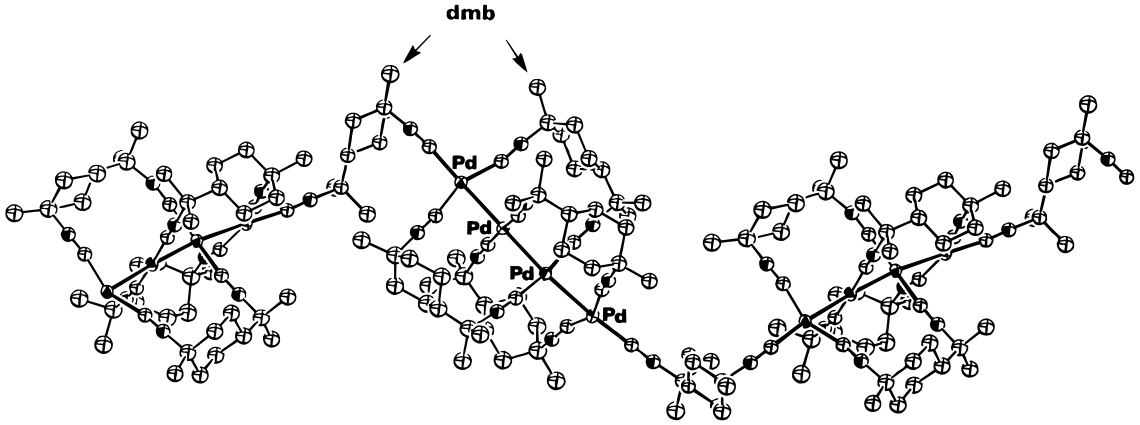

Figure 1. X-ray structure of polymer **2**. The H atoms and counteranions are omitted for clarity.

Table 1. Crystallographic Data

	2	**3**
formula	$[Pd_4(C_{12}H_{18}N_2)_5](CH_3CO_2)_2 \cdot 4H_2O$	$[Pd_2(C_{12}H_{18}N_2)_4(Cl)](C_{12}H_4N_4)_3$
fw	1503.20	1621.85
F_{000}	3208	949
space group	$P2_1/c$	$P\bar{1}$
cryst syst	monoclinic	triclinic
a, Å	19.433(2)	13.314(2)
b, Å	15.312(2)	13.490(2)
c, Å	29.156(2)	14.645(2)
α, deg	90	108.267(10)
β, deg	98.841(10)	104.834(10)
γ, deg	90	101.221(10)
Z	4	1
T, K	180(1)	293(2)
$\lambda(K\alpha_{ax})$, Å	1.540 60	1.540 60
T_{min}, T_{max}	0.7130, 0.9997	0.6578, 0.9993
V, Å^3	8572.7(1.5)	2303.8(6)
D_{calc}, g/cm^3	1.214	1.322
abs coeff, cm^{-1}	70.29	38.81
R	0.0957	0.0757
R_w	0.2932	0.2018

Table 2. Selected Bond Distances (Å) and Angles (deg) (Average Values)

	2	**3**
d(Pd−Pd)	inner = 2.597(2); outer = 2.608(2), 2.623(2)	
d(Pd−Cl)		2.7143(6)
d(Pd−C)	ax = 2.040(8); eq = 1.93(6)	1.975(9)
d(C≡N)	ax = 1.148(5); eq = 1.13(2)	1.128(5)
d(C−N)	ax = 1.482(2); eq = 1.47(2)	1.48(5)
∠(Pd_3)	175(1)	
∠(PdClPd)		180.0(1)
∠($C_{ax}Pd_2$)	174.2(6)	
∠($C_{eq}PdC_{eq}$)	162(10)	176.6(1)
∠(PdCN)	ax = 173(2); eq = 177(7)	171(1)

linearity. Although the average PdCN angle is close to linearity (177(7)°), the CPdC angle average value is somewhat smaller. The dihedral angle between the two "$Pd_2(dmb)_2^{+}$" fragments is 82.7° (local symmetry for $M_4(CN)_8$ is D_2). The slight deviation from a right angle may be due to a combination of slight inter-dmb van der Waals attractions and of crystal packing. The dmb bite distances (5.205 and 5.221 Å) are among the longest ever reported for dmb complexes (Supporting Information). While the bridging dmb ligands located on the Pd_4^{2+} moieties adopt the "typical" conformation where both −N≡C groups are oriented parallelly (U-shaped), the inter-Pd_4^{2+} dmb adopts a rarer conformation, where the $-C(CH_3)_2NC$ group rotates around the skeleton C−C single bond forming a pseudo-Z-shape. These two conformers were called rotamer-1 (U-shaped) and rotamer-2 (Z-shaped; Chart 2) in a previous paper.[4a] Examples of complexes exhibiting this Z-shaped conformer are rare. To our knowledge, this is the third example. The others were reported by us[4a] and by Che et al.,[30] in comparison with the ∼30 other compounds containing dmb in its U-shaped conformer.[10−15] The PdC distances for the axial and equatorial ligands are 2.040(8) and 1.93(6) Å on average, respectively. This difference indicates back-bonding must be less extensive at the axial positions and that the electronic density is concentrated within the Pd−Pd bonds.

Chart 2

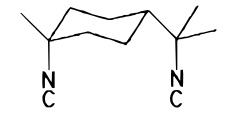

U-shape ; rotamer 1

Z-shape ; rotamer 2

The counteranions are acetate groups as expected, and there is no evidence of Cl^- ions within the lattice. This absence of Cl^- is also confirmed by X-ray fluorescence analysis. Water crystallization molecules (four per Pd_4^{2+} unit) have been located. This hygroscopic behavior is also observed for **1** as depicted in the ^{1}H NMR and IR spectra.

2. Raman Spectra. The Raman spectra are investigated for **1** for two purposes. First, the amplitudes of the PdPd interactions are addressed via the measurements of ν(PdPd) extracted in the low-frequency region of the spectra. Second, the electronic structures for the Pd_4^{2+} species are addressed experimentally using the second-moment band analysis described below. For such analysis, the knowledge of all potential candidates as Franck−Condon active modes (usually Raman active) is necessary.

The strategy for assignment of the ν(PdPd) bands is based upon comparisons with literature data for closely related Pd clusters (for which $\nu(Pd_2)$ was confirmed by resonance Raman data,[31] taking into account the M_2 bond lengths or separations[32]

(30) Xiao, H.; Cheng, K. K.; Che, C.-M. *J. Chem. Soc., Dalton Trans.* **1996**, 3699.
(31) Nakamoto, K. *Infrared and Raman Spectra of Inorganic and Coordination Compounds*, 4th ed.; Wiley: New York, 1986.

Table 3. Comparison of Spectroscopic and Structural Data for Linear and Cyclic Pd_n Clusters[a]

	assignt method	geometry	ν(M−M)/cm^{-1}	d(M−M), Å	refs
1	rel int + comp	linear	165 (a_1) 86 (a_1)	2.524(10)	this work
$Pd_3(CNCH_3)_8^{2+}$	RR	linear	166 (IR) 114 (R)	2.534(10)	*b*
$Pd_3(CNCH_3)_6(PPh_3)_2^{2+}$	RR	linear	132 (IR) 90 (R)	2.5921	*b, c*
Pd_3^-	photoelec	cyclic	230 ± 30	2.70	*d, e*
$Pd_3(dppm)_3(CO)^{2+}$	rel int + comp	cyclic	205 (a_1) 143 (e)	2.600	*f, g*
$Pd_4(dppm)_4(H)_2^{2+}$	rel int + comp	square	183 130		*h*

[a] For data on bonded and nonbonded Pd_2 species, see: Perreault, D.; Drouin, M.; Harvey, P. D. *Inorg. Chem.* **1992**, *31*, 695. RR = resonance Raman; photoelec = photoelectron spectroscopy. [b] From ref 5b. [c] From ref 5a. [d] From: Erwin, K. M.; Lineberger, W. C. *J. Chem. Phys.* **1988**, *89*, 4514. [e] Theoretical value from: Balasubramanian, K. *J. Chem. Phys.* **1989**, *91*, 307. [f] From ref 42. [g] Average value from: Manojlovic-Muir, L.; Muir, K. W.; Lloyd, B. R.; Puddephatt, R. J. *J. Chem. Soc., Chem. Commun.* **1983**, 1336. Puddephatt, R. J.; Manojlovic-Muir, L.; Muir, K. W. *Polyhedron* **1990**, *9*, 2767. [h] From data found under Supporting Information in: Gauthron, I.; Gagnon, J.; Zhang, T.; Rivard, D.; Lucas, D.; Mugnier, Y.; Harvey, P. D. *Inorg. Chem.* **1998**, *37*, 1112.

Chart 3

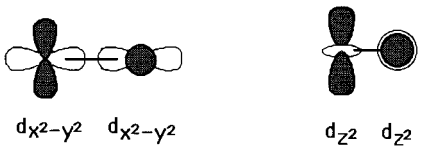

and the commonly encountered high intensities of the $\nu(M_2)$ modes. Resonance Raman spectroscopycould not be used in this work because the samples undergo severe laser damage in solutions. The two totally symmetric $\nu(Pd_2)$ modes for **1** (ν_1 = ←PM−M_2−MP→; ν_2 = ←M_2−M_2→) are readily observed at 165 and 86 cm^{-1}, respectively (Supporting Information). No other candidate for $\nu(Pd_2)$ is available below 250 cm^{-1}. These data compare very favorably with the literature (Table 3), in particular with the value for the related Pd_3^{2+} species. Using an empirical equation relating $d(Pd_2)$ in Å with the force constant $F(Pd_2)$ in mdyn Å^{-1} [10h,32]

$$d(Pd_2) = -0.387 \ln F(Pd_2) + 2.67 \qquad (1)$$

and the average $d(Pd_2)$ datum obtained for **1** (2.53 Å), we compute $F(Pd_2)$ = 1.44 mdyn Å^{-1}. The amplitude for $F(Pd_2)$ compares well with those of other binuclear systems having the same $d(Pd_2)$ values which also exhibit similar $\nu(Pd_2)$ values. **2** was not investigated since it proved to be unstable in solutions for the "time-consuming" second-moment band analysis.

3. EHMO Computations. The natures of the ground and lowest energy excited states are addressed both experimentally (section below) and theoretically. This section describes the MO picture of the linear Pd_4^{2+} cluster qualitatively since it is the first of its kind. In relation to this work, the reader should refer to the description of the ML_3 fragment in ref 33 and the work on the singly bonded $Pd_2(dmb)_2X_2$ dimers (X = Cl, Br, I),[34] including the effect of the PdL_3−PdL_3 twist angle on the MO diagram. In the latter cases, the Pd_2 σ-bonding arises from two square planar $^{\bullet}ML_3$ fragments (i.e. $^{\bullet}Pd(CNR)_2X$) interacting side-by-side mainly via the $d_{x^2-y^2}$−$d_{x^2-y^2}$ and $d_{z^2-z^2}$ interactions (Chart 3). These interactions lead to the formation of the dδ/dδ* and dσ/dσ* MO's. Due to molecular symmetry, these MO's are greatly mixed. Furthermore, the frontier orbitals (HOMO and LUMO) exhibit atomic contributions involving the Pd s and p_z orbitals, as well as some p orbitals provided by the various ligands. The present computational results are consistent with these previous works and are now described in the following way. First, the MO description of the complex $Pd_4(CNMe)_8(PH_3)_2^{2+}$ (**4**), the model for **1**, will be presented using a twist angle of 90°. Then a study of these MO's vs the twist angle will be briefly presented. Finally, model complex **5**, $Pd_4(CNMe)_{10}^{2+}$, will also be investigated and compared to **4**.

Chart 4

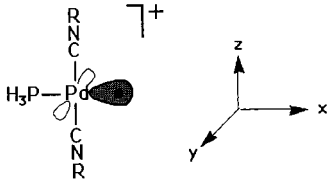

Model complex **4** can be viewed as four fragments interacting via Pd−Pd single bonds: $[H_3PPdL_2\cdots PdL_2\cdots PdL_2\cdots PdL_2PH_3]^{2+}$ where L = CNMe. The $[H_3PPdL_2^{\bullet}]^+$ fragment is isolobal with $H^{\bullet}$, $CH_3^{\bullet}$, $^{\bullet}AuPR_3$, and $^{\bullet}Mn(CO)_5$, which each possess a frontier orbital of a_1 symmetry (Chart 4). This orbital is built upon a dp hybrid pointing away from the planar T-shaped Pd fragment (C_{2v} symmetry) where the Pd atomic contributions are distributed over the d_{z^2}, $d_{x^2-y^2}$, p_x, and s orbitals. Below this orbital lie the four remaining d Pd orbitals. When this fragment interacts with the linear d^{10} PdL_2 species side-by-side as shown in Chart 3, a new fragment $[H_3PPdL_2\cdots PdL_2^{\bullet}]^+$ is generated which is also isolobal with the starting $[H_3PPdL_2^{\bullet}]^+$ fragment. The MO picture for this binuclear fragment is dominated by the Pd−Pd bonding interactions. The singly occupied a_1 frontier orbital, which arises from the dσ* MO of the Pd_2 fragment, also exhibits this dp hybrid oriented toward the missing vertex of the square planar Pd coordination. It is important to note that this frontier orbital is heavily mixed with the π-system of the CNR ligands. Such mixing is almost nonexistent for the lower energy dσ, dπ, dδ, dδ*, and dπ* MO's. The interactions between two $[Pd_2L_4(PH_3)^{\bullet}]^+$ fragments via the singly occupied a_1 hybrids generate model complex **4** ($Pd_4L_8(PH_3)_2^{2+}$). The atomic contributions and relative order for selected MO's are presented in the Supporting Information. The main computational results can be described as follows: (1) The HOMO is a filled dσ* orbital using mainly the p_x, s, d_{z^2}, and $d_{x^2-y^2}$ Pd orbitals, along with some minor p_x contributions from the P and C (isocyanide) atoms. The *x* axis is oriented parallel to the Pd−Pd bonding. (2) The LUMO is also a dσ* orbital using the

(32) $\nu(M_2)$ is a function of the force constant which can be related to the distance. Numerous empirical relationships have been proposed over the years and an account of these can be found in: Harvey, P. D. *Coord. Chem. Rev.* **1996**, *153*, 175.
(33) Albright, T. A.; Burdett, J. K.; Whangbo, M.-H. *Orbital Interactions in Chemistry*; Wiley: New York, 1985.
(34) Harvey, P. D.; Murtaza, Z. *Inorg. Chem.* **1993**, *32*, 4721.

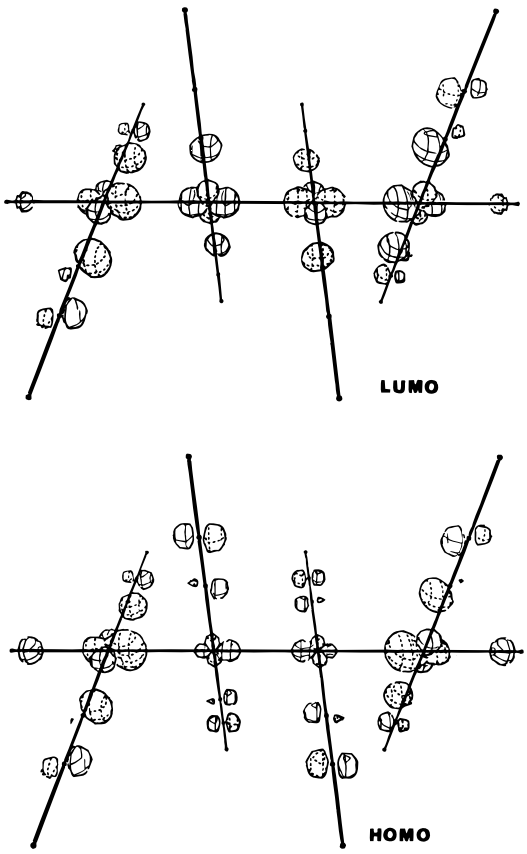

Figure 2. CACAO drawings of the LUMO and HOMO for **4**.

same atomic orbitals but with slight changes in the contributions. (3) The next 18 lower energy levels are located within ~2.5 eV and are all metal-centered MO's (details provided in the Supporting Information). (4) LUMO+1 to LUMO+4 are placed close in energy and are all π^*(CNR) orbitals. (5) Mixing between the dσ^* and dδ^* orbitals and between the dσ and dδ orbitals also occurs. Finally, both the HOMO and LUMO are relatively "well isolated" from the other MO's (~1.3 and 0.5 eV, respectively); a CACAO picture is provided in Figure 2. These large energy separations strongly predict the correct relative order of the frontier orbitals despite the qualitativeness of the computational method. This assignment is supported experimentally below.

The following series of calculations addresses the MO picture as a function of the twist angle, the twist angle being defined as the angle between the two Pd_2L_4 planes for the first and third and for the second and fourth Pd atoms. The total EHMO energy plotted against the twist angle between 90 (D_{2d} local symmetry) and 30° (D_2 local symmetry) for **4** shows an increase of 1.3 eV. However, there is very little increase in energy between 90 and 45° (~0.25 eV), and the line is essentially flat between 90 and 70°. More importantly, the MO contributions and relative MO energies undergo very little or no change in comparison with those reported in the Supporting Information. In other words, the presence of a twist angle ranging between 90 and 70° does not change the nature of the HOMO and LUMO. As the angle decreases from 45°, the total EHMO energy increases rapidly because of the close contacts of the CNR(π^*) systems and the change in dπ and dδ interactions. For smaller angles, $CH_3\cdots CH_3$ steric interactions become important and artificially increase the total energy further. These calculations are physically meaningless.

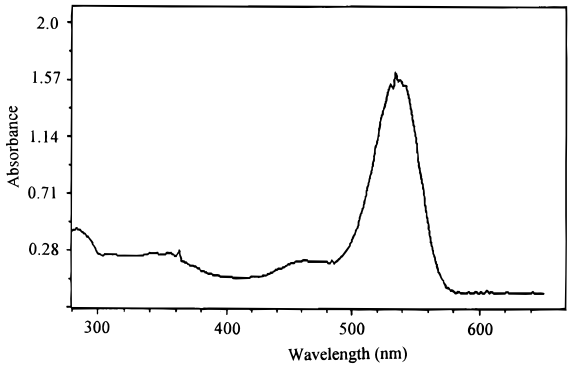

Figure 3. UV−vis spectrum of **1** in EtOH at 77 K. Note the strong and narrow band at ~500 nm (d$\sigma^* \rightarrow$ dσ^*). The solution concentration at 298 K is 1.85×10^{-5} M.

The last series of computations deals with model complex **5** in order to check whether any significant differences are present between the two different axially substituted tetramers. Structurally, a small increase in Pd−Pd bond distances has been noticed upon going from **1** (2.53 Å average value) to **2** (2.61 Å average value). There is essentially no or very little perturbation on the MO energies and the relative atomic contributions except, of course, that the axial ligand is different. More importantly the natures of the frontier orbitals are the same, i.e., π^*(CNR) > dσ^* (LUMO) > dσ^* (HOMO) > dσ, dδ mixed (HOMO−1).

4. UV−Vis Spectra and Moment Band Analysis. The electronic spectra are characterized by a strong and narrow absorption in the visible region (Figure 3) and have some similarities with the absorption spectra of other M−M-bonded quasi-linear trimers.[35] To provide a reliable assignment for these low-energy electronic bands, one should consider the ϵ data, shapes, and behavior with temperature. Absorption bands arising from the M-centered d$\sigma \rightarrow$ dσ^* transitions in M_2 σ-bonded species or from d$\sigma^* \rightarrow$ pσ transitions in M_2 face-to-face and non-M_2-bonded dimers generally undergo a significant decrease in fwhm (full width at half-maximum) upon lowering the temperature. The literature shows numerous examples for this phenomenon (d^7-d^7 and d^9-d^9 σ-bonded M_2 compounds, see refs 34, and 36, 37; for d^8-d^8 and $d^{10}-d^{10}$ compounds, see refs 38−40). This fwhm variation is due to the presence of low-frequency Franck−Condon active vibrational modes, which upon warming allow the population of vibrationally excited levels in the ground state to give rise to "hot bands" in the spectra following a Boltzmann distribution. Hence, upon cooling of the samples, the "excited" levels become less populated and fwhm decreases. For M_2 species, such modes are generally ν-(M_2) and on some occasions ν(ML) if L is heavy or weakly bonded (so ν(ML) is small) and, of course, are active in the Franck−Condon term. A good description of this phenomenon can be found in ref 40. Higher energy modes can also be Franck−Condon active, but there would not be a significant change in fwhm with temperature. For **1** (in EtOH), the data are as follows: T = 298K, λ_{max} = 538 nm or 18 600 cm^{-1}, fwhm = 2460 cm^{-1}, ϵ = 53 700M^{-1} cm^{-1}; T = 77 K, λ_{max} =

(35) Balch, A. L.; Catalano, V. J.; Chatfield, M. A.; Nagle, J. K.; Olmstead, M. M.; Reedy, P. E., Jr. *J. Am. Chem. Soc.* **1991**, *113*, 1252.
(36) Harvey, P. D.; Johnston, P.; Coville, N. J. *Can. J. Chem.* **1994**, *72*, 2176 and references therein.
(37) Harvey, P. D.; Butler, I. S.; Barreto, M. C.; Coville, N. J.; Harris, G. W. *Inorg. Chem.* **1988**, *27*, 639 and references therein.
(38) Harvey, P. D.; Gray, H. B. *J. Am. Chem. Soc.* **1988**, *110*, 2145.
(39) Piché, D.; Harvey, P. D. *Can. J. Chem.* **1994**, *72*, 705.
(40) Miskowski, V. M.; Smith, T. P.; Loehr, T. M.; Gray, H. B. *J. Am. Chem. Soc.* **1985**, *107*, 7925 and references therein.

536 nm or 18 700 cm^{-1}, fwhm = 1560 cm^{-1}. This change in fwhm is remarkable, and these data are clearly consistent with the EHMO predictions which favor the Pd-centered $d\sigma^* \rightarrow d\sigma^*$ lowest energy electronic transition.

To quantify this temperature effect, and to provide further support for this assignment, a moment analysis is performed.[41] For a fully allowed electronic transition, the oscillator strength is formally temperature independent (i.e., the area under the electronic band is constant with temperature). However, both the normalized first ($\bar{\nu}_{max}$ in cm^{-1}) and second moments ($m^2 = (8 \ln 2)^{-1}(\text{fwhm})^2$) are temperature dependent. Assuming that the bands are of Gaussian shape, then both follow a temperature dependence of the form

$$\bar{\nu}_{max} \quad \text{and} \quad m^2 = \sum_i A_i \coth\left(\frac{\hbar\omega_i}{2kT}\right) + B \qquad (2)$$

where k is the Boltzmann constant, T is the temperature, and $\hbar\omega_i$ are the ground-state vibrational frequencies for an absorption spectrum (later called $\hbar\omega_{gi}$). The temperature-independent B term in the first-moment equation is related to the electronic transition energy. The B value for the second moment should be either zero or very small, according to theory.[41] For nonzero B values, it has been proposed[40] that they be attributed to high-frequency Franck−Condon active modes which are too energetic to contribute strongly to the temperature dependence.

The UV−vis spectra vs T show a progressive change in both $\bar{\nu}$ and $(\text{fwhm})^2$ (Supporting Information). Preliminary attempts to describe both parameters and their dependence on T with a single Franck−Condon active mode (see eq 2) did not lead to satisfactory fits of the experimental data. This result indicates that two or more vibrational modes must be used in this analysis. Such an observation is not surprising since there are more than one potential candidates as Franck−Condon active modes within the $Pd_4(PPh_3)_2^{2+}$ chromophore. Indeed, a recent and similar study on the cyclic trinuclear $Pd_3(dppm)_3CO^{2+}$ cluster (dppm = $((C_6H_5)_2P)_2CH_2$) showed that both ν(PdPd) a_1 and e modes were Franck−Condon active in the lowest energy absorption.[42] The following attempts involve the use of two modes. In this case, eq 2 becomes

$$\bar{\nu}_{max} = A_1 \coth\left(\frac{\hbar\omega_{g1}}{2kT}\right) + A_2 \coth\left(\frac{\hbar\omega_{g2}}{2kT}\right) + B \qquad (3)$$

The fit becomes significantly better and the best fit is obtained for $A_1 = -6$ cm^{-1}, $\hbar\omega_1 = 165$ cm^{-1}, $A_2 = -0.66$ cm^{-1}, $\hbar\omega_2 = 86$ cm^{-1}, and $B = 1.93 \times 10^4$ cm^{-1} for the data presented in Figure 4. Changes in $\hbar\omega_1$ and $\hbar\omega_2$ of more than 10% lead to unacceptable fits. Furthermore, when parameters A_1, A_2, and B are modified slightly, the fits again become unacceptable, and the uncertainties obtained for $\hbar\omega_1$ and $\hbar\omega_2$ increase greatly. By use of a three-mode model, the uncertainties decrease only slightly (within 10%), and the three so-called "frequencies" range from 200 to 80 at best fits. The Raman spectra in this spectral window show only two scatterings. With these observations, the temperature dependence for $\bar{\nu}_{max}$ is best explained by a dominant two Franck−Condon active mode model. The assignments for these modes are trivial; $\hbar\omega_1 = \nu_1$(PdPd) a_1 and $\hbar\omega_2 = \nu_2$(PdPd) a_1. Therefore this strong absorption at ~550 nm definitely arises from a metal-centered electronic transition (i.e., $d\sigma^* \rightarrow d\sigma^*$), which is consistent with the EHMO predictions.

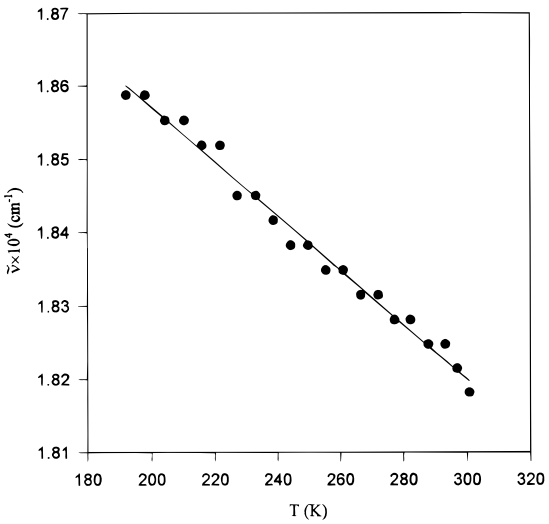

Figure 4. Graph of $\bar{\nu}_{max}$ vs T for **1** in ethanol.

For the second-moment band analysis, eq 2 becomes

$$\frac{(\text{fwhm})^2}{8 \ln 2} = A_1 \coth\left(\frac{\hbar\omega_{g1}}{2kT}\right) + A_2 \coth\left(\frac{\hbar\omega_{g2}}{2kT}\right) + B \qquad (4)$$

According to theory, $A_i = S(\hbar\omega_{ei})^2$, where S is the unitless Huang−Rhys parameter[43] and $\hbar\omega_{ei}$ is the excited-state frequency. Since fwhm is measured in cm^{-1} units, then A is in cm^{-2} units and $\hbar\omega_e$ becomes ν_e in cm^{-1} as well. The parameter S is then related to the excited-state distortion, ΔQ, according to[41]

$$S_i = \left(\frac{\mu_i \omega_e^2}{2\hbar\omega_g}\right)(\Delta Q)^2 \qquad (5)$$

where μ_i is the reduced mass of the vibrating fragments.

By converting the frequencies ω_i (s^{-1}) into ν_i (cm^{-1}) using $\omega_i = 2\pi c\nu_i$ and assuming that the ratio ν_1/ν_2 is constant for both the ground and excited states, we can rewrite eq 4 as

$$(\text{fwhm})^2 = A'\left[\coth\left(\frac{0.72\nu_{g1}}{T}\right) + K^3\left(\frac{\mu_2}{\mu_1}\right)\coth\left(\frac{0.72\nu_{g2}}{T}\right)\right] + B' \qquad (6)$$

where

$$A' = 16\pi^2(\ln 2)(\Delta Q)^2 \nu_{e1}^4 \left(\frac{\mu_1 c}{h\nu_{g1}}\right) \qquad (7)$$

$$K = \nu_{g2}/\nu_{g1} \qquad (8)$$

$$B' = B(8 \ln 2) \qquad (9)$$

The analysis was performed in two ways. First, ν_{g1} and ν_{g2} were assumed to be 165 and 86 cm^{-1}, respectively, to extract the slope and intercept for eq 6. The data are reported and compared in Table 4. Second, the parameters A, B, and ν_{g1} were set as variables, and at best fit (Figure 5) the data are for $A' = 3.06 \times 10^6$ cm^{-2}, $B' = 2.28 \times 10^6$ cm^{-2}, $\nu_{g1} = 165$ cm^{-1}, and $\nu_{g2} = 86$ cm^{-1}. These parameters compare favorably with those for other Pd_n^{2+} species (Table 4). Some brief comments can be

(41) (a) Markham, J. J. *Rev. Mod. Phys.* **1959**, *31*, 956. (b) Ballhausen, C. J. *Molecular Electronic Structures of Transition Metal Complexes*; McGraw-Hill: New York, 1979; pp 132−135.
(42) Harvey, P. D.; Hubig, S. M.; Ziegler, T. *Inorg. Chem.* **1994**, *33*, 3700.
(43) Huang, K.; Rhys, A. *Proc. R. Soc. London* **1958**, *A204*, 406.

Table 4. Comparison of the First- and Second-Moment Band Analyses for Various Pd_n^{2+} Species

			first moment			second moment		
	$\hbar\omega_1$, cm^{-1}	$\hbar\omega_2$, cm^{-1}	A_1, cm^{-1}	A_2, cm^{-1}	$10^{-4}B$, cm^{-1}	$10^{-5}A$,[a] cm^{-2}	$10^{-5}B$,[a] cm^{-2}	ref
1	165	86	−6.0	−0.66	1.93	5.48	4.11	this work
$Pd_3(dppm)_3(CO)^{2+}$	190[c]	140[c]	−210	−150	2.27	9.38	···[b]	42
$Pd_2(dmb)_2Cl_2$	175[d]		−607		2.54	6.45	1.50	34
$Pd_2(dmb)_2Br_2$	120[e]		−518		2.44	2.71	0.65	34

[a] Note that the *A* and *B* values are extracted from the graph of (fwhm)^2 vs the coth function, where the slope and the intercept have been divided by 8 ln 2. [b] This value is very small. [c] The vibrational frequencies obtained by Raman spectroscopy are 205 and 143 cm^{-1}, respectively. [d] Raman datum: 174 cm^{-1}. [e] Raman datum: 131 cm^{-1}.

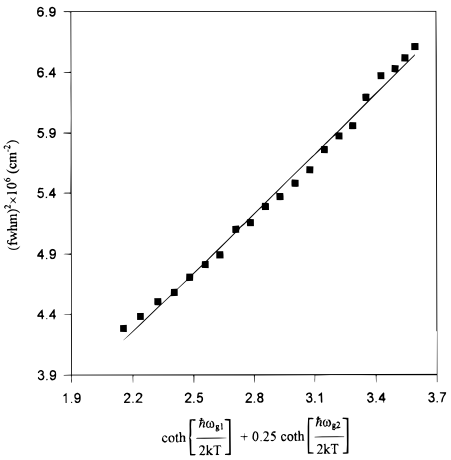

Figure 5. Graph of (fwhm)^2 vs [coth($\hbar\omega_{g1}/2kT$) + 0.25 coth($\hbar\omega_{g2}/2kT$)] for **1** in ethanol.

Table 5. ν_{e1} vs ΔQ Data[a]

ν_{e1}, cm^{-1}	ΔQ, Å	ν_{e1}, cm^{-1}	ΔQ, Å	ν_{e1}, cm^{-1}	ΔQ, Å
165	0.148	150	0.179	135	0.221
160	0.157	145	0.191	130	0.238
155	0.167	140	0.205		

[a] Calculated using eq 7.

made on this comparison. Parameter *B* (second moment) for the linear complexes appears to be dependent upon the mass of the axially coordinated ligand; i.e., the greater *B* is, the smaller the atomic mass will be (P < Cl < Br). This observation is consistent with the literature proposal that *B* is related to higher frequency Franck−Condon active modes which are too energetic to contribute strongly to temperature dependence.[40] Indeed ν(PdX) varies as X = P (270 cm^{-1}; Supporting Information) > X = Cl (240 cm^{-1})[34] > X = Br (194 cm^{-1}).[34] Parameter *A* (second moment) is greater for the larger ν_{g1}. This observation is consistent with eq 7 where $A \propto \nu_{ei}^4$. If ν_{g1} is large, then ν_{ei} is expected to be large as well, assuming that ΔQ is comparable for all systems.

Equation 7 allows for computation of ν_{e1} vs ΔQ (Table 5). In other words the calculated (fwhm)^2 is constant for all data and does not allow for extraction of ΔQ, at this point.

To simulate the absorption spectrum of **1**, Heller's time-dependent theory (which is equivalent to a traditional Franck−Condon analysis) is used.[25] The time-dependent formulation of Heller's theory applied to electronic spectroscopy involves the use of wave functions which include both the electronic transition moment between two Born−Oppenheimer potential surfaces and the ground-state vibrational wave functions. For absorption spectra, the wave functions are displaced in the wave packet and evolve with time according to the time-dependent Schrödinger equation. The overlap between the wave functions at $t = 0$ and at $t = t$ is Fourier transformed in order to obtain

Table 6. Electronic Spectral Data for **1** and **2** (77 K)

	λ_{abs}, nm		λ_{em}, nm		fwhm, cm^{-1}		τ_e, μs	
	BuCN	EtOH	BuCN	EtOH	BuCN	EtOH	BuCN	EtOH
1	532	534	685	684	2420	2520	0.56 ± 0.01	0.67 ± 0.02
2	490	488	703	698	2850	2800	1.00 ± 0.02	1.14 ± 0.05

the spectrum. Since the absorption dσ^* → dσ^* band for **1** is vibrationally unstructured, a number of scenarios listed in Table 5 must be computed. By use of $\Gamma = 1 \times 10^{-12}$ s, a position of the 0−0 band of 17 200 cm^{-1}, and a vibrational bandwidth of 80 cm^{-1}, the simulated spectra exhibit fwhm's of ∼800−900 cm^{-1} that do not vary with ΔQ. The latter behavior was expected since the injected data were extracted from eq 7. Upon an increase in the vibrational bandwidth to 200 cm^{-1}, the fwhm of the computed bandwidth increases to ∼1200 cm^{-1}. Clearly, the experimental fwhm (1560 cm^{-1}) is not reached with this simple model, because the temperature-independent contribution (B(8 ln 2)) is ignored in these first calculations. The most appropriate "high-energy" mode is the symmetric ν_1(PdP) (observed at 270 cm^{-1} in the Raman spectra; Supporting Information). This mode is selected because the P atoms contribute significantly to the LUMO and HOMO according to the EHMO model. By use of a three-mode model, for instance, $\nu_1 = 165$ cm^{-1}, $\nu_2 = 86$ cm^{-1} with $\Delta Q = 0.148$ Å (Table 5), and $\nu_3 = 270$ cm^{-1} with $\Delta Q' \sim 0.1$ Å ($\Delta Q'$ = excited distortion along the Pd−P bonds), $\Gamma = 1 \times 10^{12}$ s, and a vibrational bandwidth of 80 cm^{-1}, the simulated spectrum gives fwhm = 1400 cm^{-1}. This result represents a drastic improvement of the model. By a subsequent increase in both the vibrational bandwidth and $\Delta Q'$, the experimental value for fwhm (1560 cm^{-1}) is easily reached. Any further analysis is futile at this point since $\Delta Q'$ for this temperature-independent term and the vibrational bandwidth are unknown. Nonetheless, the absorption band is clearly best described by a three-mode model, two that are temperature dependent (hot bands) and one that leads to an independent contribution to the fwhm. Intricate details of this analysis can only be provided for the cases where fine structure could be observed.

On the basis of the EHMO model computed for the LUMO and HOMO, the change in bond order (BO) for an M_4 complex with an excited electronic configuration (dσ^*)^1(dσ^*)^1 should, in theory, be nil. However, a close examination of the HOMO and LUMO atomic contributions shows more "negative overlaps" in the Pd−Pd bonding in the LUMO than in the HOMO, and therefore, the LUMO appears somewhat more Pd−Pd antibonding than the HOMO. Hence, the ΔQ values in Table 5 should be treated as bond lengthening. With the assumption that ΔQ is 0.148 Å (first entry in Table 5), the average Pd−Pd distance in **1** increases to 2.67 Å (2.524 Å[29] + 0.148 Å). This value is still reasonable for a Pd_4 system with some Pd−Pd bonding. Under these conditions, this electronic configuration imposes a dmb bite distance of 5.34 Å. Such a distance can

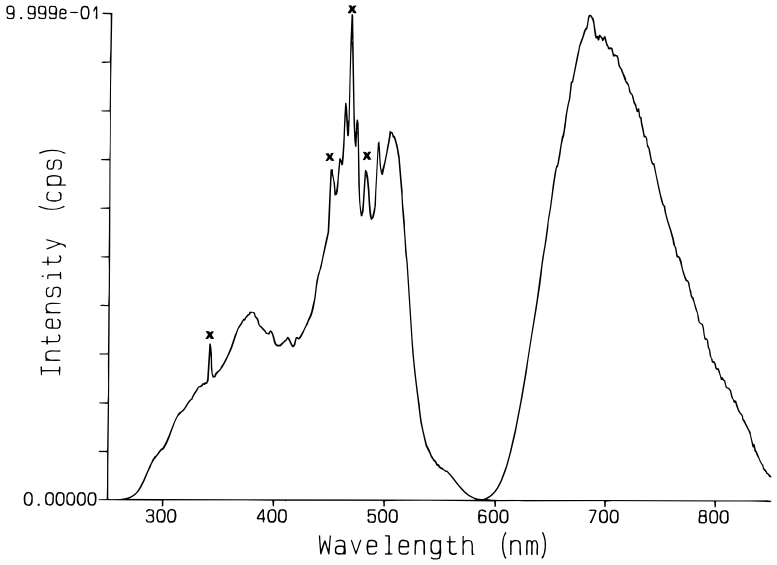

Figure 6. Emission spectrum of **1** in EtOH at 77 K.

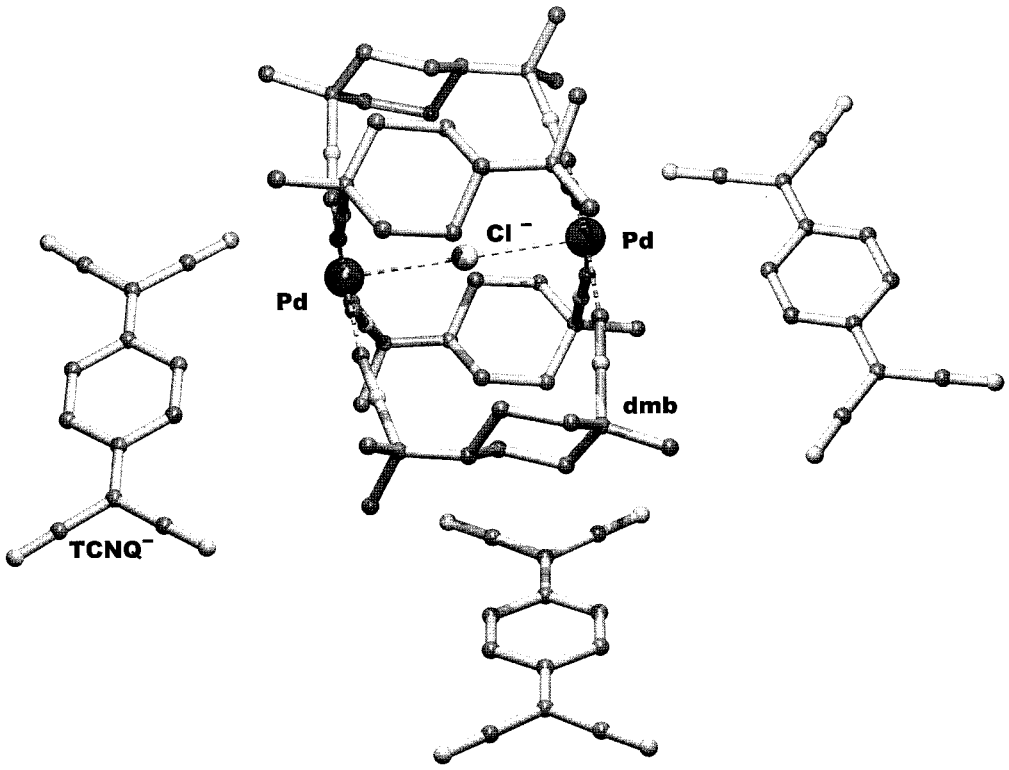

Figure 7. ORTEP drawing of **3**. The atoms are represented with 50% probability ellipsoids, and the H atoms and $TCNQ^-$ ions are omitted for clarity.

easily be accommodated by dmb since the longest bite distance known for dmb is 5.428(2) Å for **3** (Supporting Information; discussed below).

5. Emission Spectra. Both **1** and **2** are not luminescent at room temperature but are at 77 K in glass matrixes (see Table 6 and Figure 6 for examples). Both exhibit emission lifetimes in the 0.5−1.2 μs range, and the energy gap between the absorption and emission maxima are 4100 and 5750 cm^{-1} for **1** and **2**, respectively. These long lifetimes indicate that the luminescence is phosphorescence and are assigned to a $d\sigma^* \rightarrow d\sigma^*$ spin-forbidden photoprocess. Furthermore, these emission bands are vibrationally unstructured. The fwhm values (2400 cm^{-1} < fwhm < 2850 cm^{-1}) are somewhat large and suggest that ΔQ is large as well. This observation is consistent with the EHMO model, which classifies the HOMO $d\sigma^*$ as somewhat less Pd−Pd antibonding than the LUMO $d\sigma^*$.

The emission lifetimes for the weakly emitting d^9-d^9 $Pd_2(dmb)_2X_2$ complexes are 0.071 (X = Cl) and 0.177 μs (X = Br) at 77K (solvent = EtOH),[10i] and that for the strongly luminescent d^{10}−d^{10} $Pd_2(dppm)_3$ complex is 107 μs (solvent = 2-methyltetrahydrofuran; T = 77 K).[44] Compounds **1** and **2** are somewhat weakly luminescent, and their emission lifetimes compare more favorably to those of the singly bonded d^9−d^9 dimers ($Pd_2(dmb)_2X_2$ and $Pd_2(tmb)_2X_2$; tmb = 2,5-dimethyl-2′,5′-diisocyanohexane; X = Cl, Br). The low τ_e values for the d^9−d^9 species were interpreted in terms of efficient homolytic

(44) Harvey, P. D.; Gray, H. B. *J. Am. Chem. Soc.* **1988**, *110*, 2079.

Pd−Pd and Pd−X bond cleavage in the excited states, somewhat similar to that described by Metcalf and Kubiak for the $Pd_2(CNCH_3)_6^{2+}$ dimer.[45] It is anticipated that the relatively low excited-state lifetimes for **1** and **2** are related to same photophysical processes (i.e., photoinduced cleavage of the Pd−Pd bond and labilization of the axial ligands).

6. Preparation of 3. In an attempt to prepare a polymeric material of the type $\{Pd_4(dmb)_5^{2+}\}_n\{2TCNQ^-\}_n$ as a precursor for the mixed valence $\{[Pd_4(dmb)_5^{2+}](TCNQ^-)_2 \cdot xTCNQ^0\}_n$ material as a potential electric conductor, complex **3** was made unexpectedly. According to the preparation of **1** and **2**, the reaction of $Pd_2(dba)_3$ with dmb in the presence of an oxidizing agent ($CHCl_3$ or CH_2Cl_2; $Pd^{II}(O_2CCH_3)_2$) generates the "$\{Pd_4(dmb)_5^{2+}\}_n$" species, which can remain as a polymer (**2**) or segment with a slight excess of PPh_3 (to produce **1**). This same reaction in the presence of an excess of $TCNQ^0$ as an oxidizing agent leads to compound **3** instead. In this case, the expected mixed-valence "Pd_4^{2+}" species are not isolated since the oxidation process is pushed toward the formation of a binuclear d^8-d^8 species.

The interest in this compound arises mostly from the prediction made several years ago by Gray et al.[15] on the basis of spectroscopic observations that the encapsulation of halide ions is possible by the "$Pd_2(dmb)_4^{2+}$" species. To our knowledge, the X-ray structure of **3** is the first formally characterized example of this type (windmill structure "$M_2(dmb)_4$") containing the fragment M−X−M (Figure 7; Tables 1 and 2). d(Pd···Cl) is 2.7143(6) Å (∠PdClPd = 180.0(1)°), which corresponds to a rather ionic bonding and places the dmb bite distance at 5.428 Å, the longest one ever reported for the dmb ligand. The d(Pd−C), d(C≡N), and d(C−N) data are normal, and the CPdC (176.6(1)°) and PdCN (171.2(1.1)°) angles deviate slightly from linearity. $TCNQ^-$ acts as a simple counteranion where no π-stacked chain is observed.[46]

The preparation of new polymeric materials of the type $\{[M^+(dmb)_2]TCNQ^- \cdot xTCNQ^0\}_n$ (M = Cu, Ag) exhibiting both electric conductivity and photoconductivity will be reported in due course.[47]

Acknowledgment. This research was supported by the Natural Sciences and Engineering Research Council and by the Fonds Concerté pour l'Avancement de la Recherche.

Appendix

The equation relating the second moment to two Franck−Condon active modes in an allowed electronic transition is

$$\frac{(\text{fwhm})^2}{8\ln 2} = \sum_i A_i \coth\left(\frac{\hbar\omega_i}{2kT} + B\right)$$

For an absorption spectrum, ω_i becomes ω_{gi} (ground state). With $A_i = S_i(\hbar\omega_{ei})^2$ and $i = 2$ modes, the equation becomes

$$\frac{(\text{fwhm})^2}{8\ln 2} = S_1(\hbar\omega_{e1})^2 \coth\left(\frac{\hbar\omega_{g1}}{2kT}\right) + S_2(\hbar\omega_{e2})^2 \coth\left(\frac{\hbar\omega_{g2}}{2kT}\right) + B$$

Because fwhm is in cm^{-1} units, A_i is in cm^{-2} and $\hbar\omega_{ei}$ becomes ν_{ei} in the expression $A_i = S_i(\hbar\omega_{ei})^2$ (e = excited state). Using the equation

$$S_i = \left(\frac{\mu\omega_{ei}^2}{2\hbar\omega_{g1}}\right)(\Delta Q)^2$$

the above equation can be rewritten as

$$\frac{(\text{fwhm})^2}{8\ln 2} = \nu_{e1}^2\left(\frac{\mu\omega_{e1}^2}{2\hbar\omega_{g1}}\right)(\Delta Q)^2 \coth\left(\frac{\hbar\omega_{g1}}{2kT}\right) + \nu_{e2}^2\left(\frac{\mu\omega_{e1}^2}{2\hbar\omega_{g2}}\right)(\Delta Q)^2 \coth\left(\frac{\hbar\omega_{g2}}{2kT}\right) + B$$

To convert ω (s^{-1}) to ν (cm^{-1}) for the remainder of the demonstration, we use $\omega_i = 2\pi c\nu_i$ (c = speed of light). Furthermore, by replacing $\hbar$ and k by their respective values, we obtain

$$\frac{\hbar\omega_{gi}}{2kT} = \frac{0.72\nu_{gi}}{T}$$

where ν_{gi} is in cm^{-1} and T is in kelvins. Upon multiplication by 8 ln 2, the equation becomes

$$(\text{fwhm})^2 = 16\pi^2(\ln 2)(\Delta Q)^2\nu_{e1}^4\left(\frac{\mu_1 c}{h\nu_{g1}}\right)\coth\frac{0.72\nu_{gi}}{T} + 16\pi^2(\ln 2)(\Delta Q)^2\nu_{e2}^4\left(\frac{\mu_2 c}{h\nu_{g2}}\right)\coth\frac{0.72\nu_{g2}}{T} + B(8\ln 2)$$

For μ_1, we consider ν_1, which is approximated by $P-\overleftarrow{Pd}-\overrightarrow{Pd}-\overleftarrow{Pd}-\overrightarrow{Pd}-P$, and for μ_2, we consider ν_2, which is approximated by $\overleftarrow{Pd}-\overrightarrow{Pd}-\overleftarrow{Pd}-\overrightarrow{Pd}$. Hence

$$\mu_1 \sim \frac{m_{PdP}m_{Pd}}{m_{PdP} + m_{Pd}}$$

$$\mu_2 \sim \frac{m_{Pd_2}m_{Pd_2}}{m_{Pd_2} + m_{Pd_2}}$$

By assuming that the ratio ν_2/ν_1 is constant for both the ground and excited states since the geometry does not change significantly, we have

$$\nu_2 = K\nu_1$$

$$\nu_2^4 = K^4\nu_1^4$$

By replacing ν_2 in the equation for $(\text{fwhm})^2$, we obtain

$$(\text{fwhm})^2 = 16\pi^2(\ln 2)(\Delta Q)^2\nu_{e1}^4\left(\frac{\mu_1 c}{h\nu_{g1}}\right)\left[\coth\left(\frac{0.72\nu_{g1}}{T}\right) + \left(\frac{\mu_2}{\mu_1}\right)K^3\coth\left(\frac{0.72\nu_{g2}}{T}\right)\right] + B(8\ln 2)$$

Hence a graph of

$$(\text{fwhm})^2 \quad \text{vs} \quad \left[\coth\left(\frac{0.72\nu_{g1}}{T}\right) + \left(\frac{\mu_2}{\mu_1}\right)K^3\coth\left(\frac{0.72\nu_{g2}}{T}\right)\right]$$

gives a slope of $A = 16\pi^2(\ln 2)(\Delta Q)^2\nu_{e1}^4(\mu_1 c/h\nu_{g1})$ and an

(45) Metcalf, P. A.; Kubiak, C. P. *J. Am. Chem. Soc.* **1986**, *108*, 4682.
(46) Miller, J. S.; Epstein, A. J. Synthesis and Properties of Low-Dimensional Materials. *Ann. N.Y. Acad. Sci.*, **1978**, *313*.
(47) A preliminary account of this work has appeared: Fortin, D.; Harvey, P. D. *Proc. 12th ISPPCC Cond. Chem. Rev.* **1998**, *171*, 351.

intercept of $B(8 \ln 2)$. If $\nu_{g1} = 165$ cm^{-1} and $\nu_{g2} = 86$ cm^{-1}, then $K^3 = 0.14(\mu_2/\mu_1) = 0.25$.

Supporting Information Available: Tables giving crystal data, structure refinement details atomic coordinates, bond lengths and angles, anisotropic displacement parameters, hydrogen coordinates and isotropic displacement parameters, and torsion angles for **2** and **3**, a comparison of dmb bite distances, and EHMO atomic contributions for $Pd_4(CNMe)_8(PH_3)_2^{2+}$, an additional structural diagram of **2**, an FT-Raman spectrum of **1**, UV−vis spectra of **1** in EtOH as a function of temperature, and X-ray crystallographic files, in CIF format, for **2** and **3**. This material is available free of charge on the Internet at http://pubs.acs.org.

IC9811594